Homogeneous nucleation rate measurements in supersaturated water vapor II

David Brus,[1,2,a)] Vladimír Ždímal,[1] and Hermann Uchtmann[3]
[1]*Laboratory of Aerosol Chemistry and Physics, Institute of Chemical Process Fundamentals AS CR, v.v.i., Rozvojová 135, CZ-16502 Prague, Czech Republic*
[2]*Finnish Meteorological Institute, Erik Palménin aukio 1, P.O. Box 503, FI-00101 Helsinki, Finland*
[3]*FB Chemie, Institute of Physical Chemistry, Philipps-University Marburg, D-35032 Marburg, Germany*

(Received 3 June 2009; accepted 3 August 2009; published online 21 August 2009)

The homogeneous nucleation of water was studied experimentally in this work using a thermal diffusion cloud chamber; droplets were counted by the photomultiplier method and helium was used as a carrier gas. The nucleation rates range from 3×10^{-2} to 3×10^{1} cm^{-3} s^{-1} and six isotherms from 295 to 320 K with step of 5 K are measured. The experimental setup and obtained data are mutually compared to our previous publication [Brus *et al.*, J. Chem. Phys. **129**, 174501 (2008)], where the droplets were counted using digital photography and image processing. The molecular content of the critical clusters was estimated from the slopes of experimental data. The measured isothermal dependencies of the nucleation rate of water on the saturation ratio were compared with previously published data of others, several theoretical predictions, and the former nucleation onset data. The aim of the present investigation was to show for the first time that nucleation results can be quantitatively reproduced with two different experimental setups operated in different ways. © *2009 American Institute of Physics*. [DOI: 10.1063/1.3211105]

I. INTRODUCTION

There is no other substance on Earth whose properties have been studied in such detail as the properties of water. One of the key conditions for life on Earth is the hydrological cycle; the critical step of this cycle is condensation of water. Compared to condensation, none of the other processes involved in the cycles require overcoming an energetic barrier that high, even though the aerosol particles—always present in the troposphere in sufficient concentrations—lower this barrier substantially. When these heterogeneous nuclei are removed together with charged clusters, the energetic barrier needed to be overcome increases dramatically. This process of forming liquid water embryos only by mutual collisions of water molecules is termed homogeneous nucleation.

The first attempt to study homogeneous nucleation quantitatively was that of Wilson (1897) more than 100 years ago.[1] Since then, many authors followed using more and more sophisticated experimental setups and trying to more open the window of available operating conditions. Until the 1970s, all these attempts focused on determining the so-called critical supersaturation or "onset of condensation," meaning conditions when the newly formed condensed phase starts to be observed at given temperature. Various experimental approaches were developed to achieve this goal—the overview of these studies is given in Table I.

As the sensitivity of experimental methods increased, and especially after the launch of computers allowed the utilization of results of the Mie theory in practical calculations, a new boom of experimental methods started. These methods allowed to investigate the rates of nucleation much more precisely with the goal to determine the real dependence on supersaturation, while keeping the nucleation temperature constant. The overview of these refined studies on homogeneous nucleation of water is shown in Table II.

Table II depicts an interesting fact. While all other experimental approaches were successful in providing reasonable data, the thermal diffusion cloud chamber (TDCC) data were lacking until last year. The reason was described boldly in the seminal paper by Katz and Ostermier (1967),[7] who stated that "water was not condensing as a smooth film but as droplets on the upper surface." It took almost 40 years to overcome this obstacle, develop a precise method to determine the homogeneous nucleation rate and obtain consistent data on water nucleation kinetics using the TDCC.

This paper is the second one providing original experimental data on homogeneous nucleation of water obtained using a TDCC. The results differ mainly in the way the nucleation rate was determined. In the paper of Brus *et al.* (2008) (Ref. 32) a photographic method to localize and count the droplets formed by nucleation was used (Ždímal and Smolík, 1998).[33] In this work, the integral flux of droplets is counted with a photomultiplier (Marvin and Reiss, 1978) (Ref. 34) and a normalization suggested by Hung *et al.* (1989) (Ref. 35) is used to calculate the nucleation rate from the measured flux. This paper describes the improved method of droplet counting, reports its results, and compares them both directly with the results of Brus *et al.* (2008) (Ref. 32) and also indirectly to the data of others. A comparison with predictions of nucleation theory and their parametrizations is carried out as well.

a)Electronic mail: brus@icpf.cas.cz.

TABLE I. Overview of studies determining so-called critical supersaturation or onset of condensation in supersaturated water vapor.

Authors and reference	Year	Method	Inert
Wilson, Ref. 1	1897	Expansion cloud chamber	Air/O_2/N_2
Powell C.F., Ref. 2	1928	Expansion cloud chamber	Air
Volmer and Flood, Ref. 3	1934	Expansion cloud chamber	Air
Scharrer I., Ref. 4	1939	Expansion cloud chamber	Air
Sander and Damkohler, Ref. 5	1943	Expansion cloud chamber	
Madonna *et al.*, Ref. 6	1961	Expansion cloud chamber	N_2
Katz and Ostermier, Ref. 7	1967	Thermal diffusion cloud chamber	H_2
Jaeger *et al.*, Ref. 8	1969	Supersonic nozzle	Air
Stein and Moses, Ref. 9	1972	Laval nozzle	No inert
Barschdorff *et al.*, Ref. 10	1972	Supersonic nozzle	No inert
Heist and Reiss, Ref. 11	1973	Thermal diffusion cloud chamber	He/H_2
Mirabel and Katz, Ref. 12	1977	Thermal diffusion cloud chamber	He
Wegener and Lee, Ref. 13	1983	Shock tube	Ar
Chukanov and Kuligin, Ref. 14	1987	Thermal diffusion cloud chamber	He
Peters, Ref. 15	1987	Shock tube	Ar
Koppenwallner and Dankert, Ref. 16	1987	Free jet	No inert
Peters and Paikert, Ref. 17	1989	Shock tube	Ar
Heath *et al.*, Ref. 18	2002	Supersonic nozzle	No inert
Kim *et al.*, Ref. 19	2004	Supersonic nozzle	No inert

II. EXPERIMENTAL METHOD

The first TDCC and the obtained experimental data are presented in previous publication of Brus *et al.* (2008).[32] The second chamber was built and operated at Philipps-University in Marburg, Germany and will be presented here in detail. Even though the basic principle of operation is the same for both chambers, the experiments differ in the way the nucleation rate is determined.

The basic function of the TDCC is to produce supersaturated vapor by using nonisothermal diffusion. The chamber is designed so that one-dimensional diffusion of vapor takes place through an inert carrier gas. The second chamber used in this investigation consists of two circular stainless steel plates, separated by a 43 mm high and 5 mm thick glass ring with an inner diameter of 175 mm. The effective diameter to height (the distance between liquid films) ratio is 5:1. To minimize the wall effect, the ring is wrapped by four equally spaced resistance wires connected to individual power supplies. The bottom plate covered with a thin film of the studied liquid is heated. Vapor of the studied substance evaporates from the film surface, diffuses through an inert gas and condenses on the cooler top plate. The condensate flows along the glass wall back to the pool, so that the chamber can be operated at a steady state. The type and pressure of the inert gas are chosen so, that the density profile is stable against buoyancy driven convection. Under such circumstances, the character of transport processes between the plates leads to a state, where both the temperature T and the partial vapor pressure p_A decrease almost linearly with the increasing chamber height, see Fig. 1. Since the equilibrium vapor pressure p_{eq} decreases with the height more quickly than p_A, the vapor in the chamber becomes supersaturated with a maximum supersaturation $S=p_A/p_{eq}$ reached close to the top plate. By increasing the temperature difference be-

TABLE II. Overview of studies determining homogeneous nucleation rate, J as a function of supersaturation S and temperature T in supersaturated water vapor.

Authors and reference	Year	Method	Inert
Allen and Kassner, Ref. 20	1969	Expansion cloud chamber	Ar/He
Stein and Armstrong, Ref. 21	1973	Free jet	No inert
Wagner and Strey, Ref. 22	1981	Two piston expansion chamber	Ar
Miller *et al.*, Ref. 23	1983	Expansion cloud chamber	Ar
Beloded *et al.*, Ref. 24	1989	Expansion cloud chamber	Ar
Viisanen *et al.*, Ref. 25	1991	Two valve expansion chamber	He
Viisanen *et al.*, Ref. 26	1993	Two valve expansion chamber	He/Ne/Ar/Kr/Xe
Luijten *et al.*, Ref. 27	1997	Pulse expansion wave tube	N_2
Luijten *et al.*, Ref. 28	1999	Pulse expansion wave tube	He/N_2
Wölk and Strey, Ref. 29	2001	Two valve expansion chamber	Ar
Mikheev *et al.*, Ref. 30	2002	Laminar flow tube reactor	He
Holten *et al.*, Ref. 31	2005	Pulse expansion wave tube	He
Brus *et al.*, Ref. 32	2008	Thermal diffusion cloud chamber	He

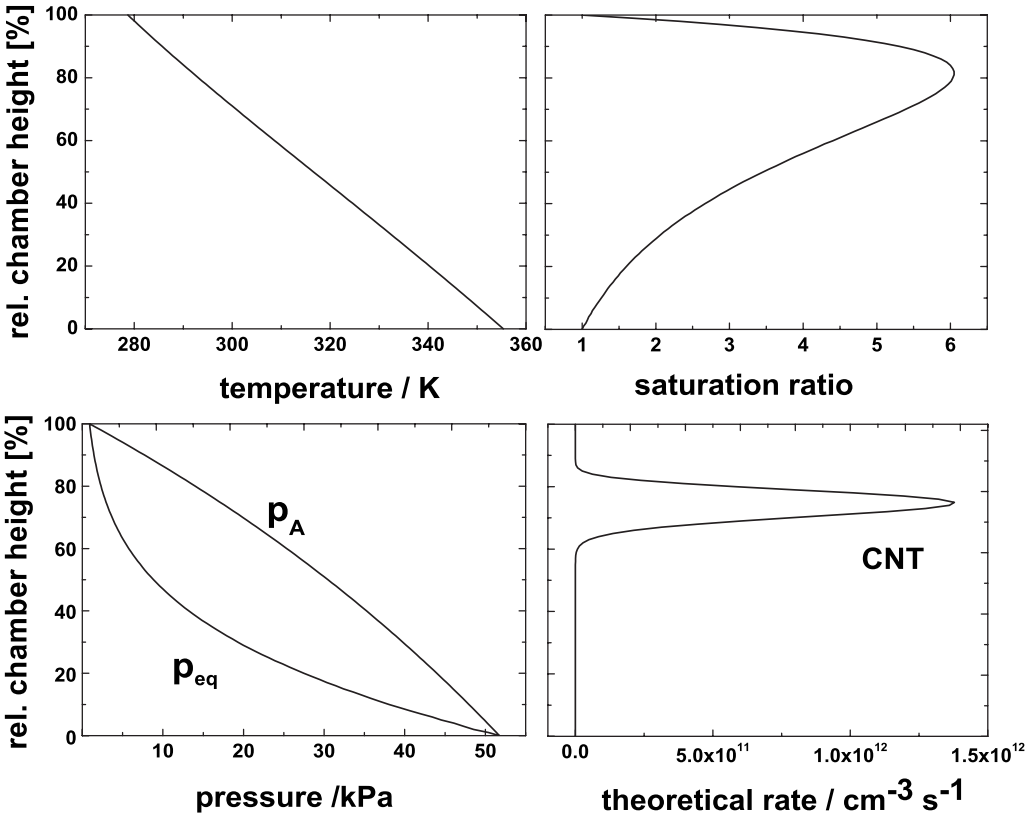

FIG. 1. Vertical profiles of temperature, partial and equilibrium vapor pressure of water, saturation ratio, and nucleation rate inside the TDCC.

tween both plates, the supersaturation can be increased until it is sufficient for homogeneous nucleation to start. Temperatures of the liquid surfaces are not measured directly but temperatures of the plates are measured instead, the temperatures of the liquid surfaces have to be calculated. It is assumed that the heat conduction is the main mechanism of heat transport through the films.[33] The self-cleaning nature of the chamber hinders heterogeneous nucleation. The nucleation induced by ions is effectively prevented by applying an electrostatic field (35 V cm^{-1}) across the chamber. Stable clusters of the new phase are formed and then grow rapidly to become visible droplets; all this happens inside a thin layer called a nucleation zone (spanning over about 10% of chamber height see Fig. 1) with the nucleation rate maximum located somewhat below the supersaturation maximum. The formed droplets fall back to the liquid film due to gravity.

The overview of dimensions and operation parameters of both chambers is given in Table III. The mathematical model describing the one-dimensional coupled heat and mass transfer in the chamber was described earlier (Katz, 1970);[36] it was later adapted for conditions of both chambers (Ždímal and Smolík, 1998) (Ref. 33) and as a result, given the boundary temperatures and total pressure in the chamber, it provides fluxes of heat and mass between the plates, and also vertical profiles of temperature, and partial pressure of the vapor and its saturation ratio. The same code was used to process results from both chambers considering minor differences in chamber geometry and other experimental parameters given above. It was shown, e.g., in Stratmann *et al.*, (2001) (Ref. 37) that the assumption of one-dimensional mass and heat flow provides a sufficient representation of transport processes in the chamber, if the operating parameters are chosen properly.

A principal problem of former investigations on water nucleation in diffusion cloud chambers was the wetting of the top plate by water. It is an essential condition, in order to operate the chamber in a steady state, that the condensing material forms liquid film on the colder top plate, in this film the liquid slowly moves toward the glass wall and flows down to the liquid pool at the bottom plate. It is especially difficult to fulfill this condition in the case of water, which has a high surface tension and tends to condense in the form of big droplets on the inner surface of the top plate. These droplets then fall down inside the chamber, disturb the otherwise calm transport processes, and make the one-

TABLE III. The overview of dimensions and operation parameters.

Chamber	Diameter (mm)	Height (mm)	Effective ratio	Temperature control bottom/top plate	Wall heating	Plate material
I	175	43	4.6	Thermostat/thermostat	Four wires	Stainless steel
II	160	25	6.7	Electrical/thermostat	Six wires	Duraluminum

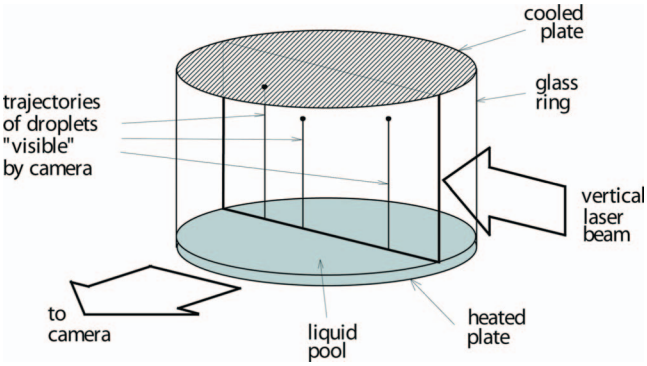

FIG. 2. Schematic figure of the photographic method.

dimensional model invalid. With the aluminum chamber it was possible to achieve its wetting by very careful cleaning and special treatment of the upper plate. Its wetting was possible because of the oxide layer always present on aluminum surfaces. In the stainless steel chamber the top plate was coated with a ceramic layer with a thickness of less that 0.1 mm. This was done by a commercial company (Schrage, GmbH) specializing in ceramic coatings. The ceramic layer consisting mainly of Al_2O_3 is absolutely resistant to water and at the same time it is easily wetted.

With the chambers operating properly the nucleation experiments were performed using two completely different and independent methods of droplet counting.

A. Method I: Photographic method

The method of precise determination of the nucleation rate is described in detail in the paper of Brus *et al.* (2005).[38] The optical system consists of a He–Ne laser, beam shaping optics, and a charge coupled device (CCD) camera. The flattened laser beam illuminates the chamber from the side over its whole height, passing through its axis. Trajectories of the droplets, formed inside this beam, are recorded by a CCD camera positioned exactly perpendicularly to the beam to record droplets trajectories on-line, see Fig. 2. Algorithms of image analysis are used to determine vertical positions of nucleated droplets on the digital images.[39] After evaluating a sufficient number of visible droplets (starting points) in one experiment, we obtain their number distribution as a function of the chamber height. By dividing the number distribution by the photographed volume and the exposure time we get the homogeneous nucleation rate (as droplets per cubic centimeter per second) as a function of the height in the chamber. The homogeneous nucleation rate distribution is subsequently fitted by a Gaussian distribution. This method presents the experimentally determined homogeneous nucleation rate, $J_{\mathrm{exp}}(z)dz$, as a function of vertical position inside the chamber, z. These local values of nucleation rate are then related to the corresponding values of temperature and supersaturation, as calculated using the one-dimensional model of mass and heat transport in the TDCC.[33,38] The resulting dependence $J_{\mathrm{exp}}(T,S)$ is directly comparable to the theoretical prediction of any nucleation theory.

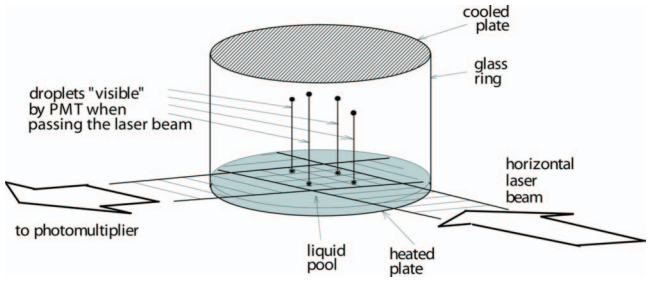

FIG. 3. Schematic figure of the integral method.

B. Method II: Integral counting

The method of integral counting uses a laser beam shaped by cylindrical optics to a thin ribbon of light (thickness of about 0.4 mm, width of 2 cm). The laser beam is positioned near the surface of the liquid pool in the chamber. The scattered light caused by drops falling through the laser beam is registered by a photomultiplier (PMT) and after discrimination the electrical pulses are counted giving the integral number of droplets formed in the chamber, see Fig. 3. The flux is given as drops per area and second.

For comparison with theory the rate given as a number of drops per cubic centimeter and second is needed. Under the assumptions given in Hung *et al.* (1989) (Ref. 35) the nucleation rate J_{exp} at a plane where the theoretical prediction J_{th} has its maximum (called the maximum rate plane) can be calculated as

$$J_{\mathrm{exp}}(\max) = \frac{\int J_{\mathrm{exp}}(z)dz}{\int J_{\mathrm{th}}(z)dz} J_{\mathrm{th}}(\max). \quad (1)$$

This is a local value of nucleation rate (drops per cubic centimeter and second) that can be related to the corresponding local values of temperature and supersaturation at the same height. Thus $J(T,S)$ is obtained that can be compared to theoretical predictions. This procedure is only weakly dependent on the theory chosen (see Hung *et al.*, 1989).[35]

1. Counting area determination

For this procedure the counting area has to be determined as exactly as possible. In the present investigation the problem has been solved by a two laser coincidence technique, see Fig. 4. Two He–Ne lasers were used for counting a green and a red one with wavelengths of 542 and 632 nm. Light scattered by the droplets is detected independently by two PMTs provided with interference filters selecting the corresponding red or green light. Special software was developed that allowed coincidence counting. Only droplets falling through the intersection of the two laser beams are counted as a droplet, because they gave simultaneous electrical pulses in both PMTs.

The discriminator electronics is the same as for one color counting. In this way, a counting area is defined very exactly by the geometry of the two laser beams, which is determined easily by measuring their corresponding width and position. The coincident count rates can be related to rates counted only by the red laser which is usually used in the nucleation experiments. The ratio of the rates gives the

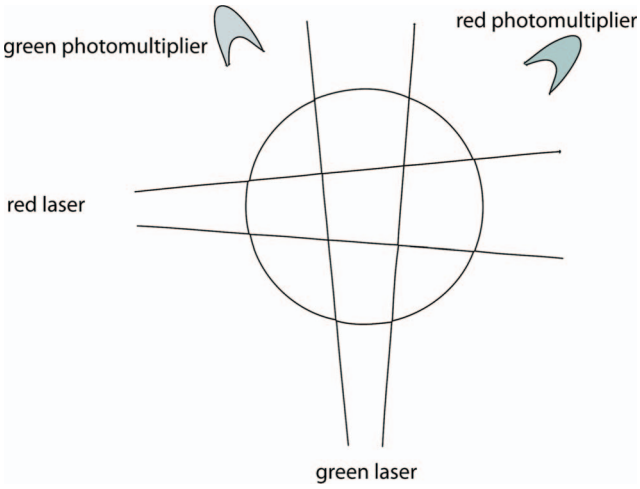

FIG. 4. Schematic figure of coincident counting.

ratio of the areas. So with an unchanged geometry the further experiment is performed with the red laser only after the calibration procedure of the counting area.

The coincidence method is also used to prove the homogeneity of the rain in the chamber by moving the counting area. The drops are evenly distributed across the chamber except for a range near the chamber wall (approximately 3 cm). This experiment justifies the applicability of area calibration for one laser counting.

In this study a purified water (ULTRAPURE, electrical conductivity $<0,1\ \mu S/cm$, TOC<10 ppb) as the condensing vapor and helium (Linde, purity 99.996%) as the carrier gas were used. The physicochemical properties of water and helium are the same as presented in Brus *et al.*, (2008).[32]

III. RESULTS AND DISCUSSION

Homogeneous nucleation rates of water in helium were measured in the range from 2×10^{-2} to 5×10^{1} $cm^{-3}\ s^{-1}$. The lower limit of the TDCC is caused by the difficulties in running very long experiments (many hours) and the higher limit due to vapor depletion and latent heat release. The nucleation temperatures studied in this paper cover the range from 295 to 320 K in steps of 5 K. The lower temperature limit is given by the fact that water should not freeze on the cooled top plate of the chamber. Theoretically, the bottom plate temperature is limited by the critical point of water; practically, its temperature is much lower limited by the condition of a "not boiling" liquid pool at the operating pressure of the chamber. The pressure in the TDCC was varied from 80 kPa at $T_{nucl}=295$ K to 125 kPa at $T_{nucl}=320$ K.

The obtained experimental nucleation rate data are presented in Table IV. The nucleation rates as a function of the saturation ratio are presented in Fig. 5. It can be seen, that the experimental data are in qualitative agreement with the prediction of the classical theory of homogeneous nucleation (CNT).[40] The experimental points of the 320 K isotherm lie just on the top of theoretical prediction. However toward the lower temperature isotherms the deviation from CNT increases.

In Fig. 6 we compare our experimental data to experimental data of Brus *et al.* (2008),[32] only corresponding isotherms are presented (320, 310, and 300 K). Also we compare our experimental data to the empirical nucleation rate function of Wölk *et al.* (2002) (Ref. 41) and scaled model of nucleation suggested by Hale.[42–44] Experimental data fits well to Hale's scaled model at nucleation temperatures 320, 310, and 300 K. The deviation from the empirical prediction of Wölk *et al.* (2002) (Ref. 41) increases toward the higher temperature isotherms, and reaches about two orders of magnitude at 320 K. Such behavior is in contradiction to data of Brus *et al.* (2008),[32] where the deviation from empirical prediction increases toward the lower temperatures.

A. Comparison with the onset measurements

In Fig. 7 the data of this work are compared to the onset measurements of Wilson (1897),[1] Volmer and Flood (1934),[3] Heist and Reiss (1973) (Ref. 11) (separately for both carrier gases hydrogen and helium), Peters (1987),[15] Mirabel and Katz (1977),[12] and of Chukanov and Kuligin (1987) (Ref. 14) and Brus *et al.* (2008).[32] The ratio of the onset saturation ratio to the saturation ratio predicted by CNT theory is plotted as a function of the nucleation temperature. We have chosen the ratio S_{exp}/S_{CNT} on the vertical axis because Fig. 4 presents a combination of data obtained from both the expansion and the diffusion based devices, each of them using another value of the onset nucleation rate: e.g., Peters (1987) (Ref. 15) takes 10^{11} $cm^{-3}\ s^{-1}$ while this work uses data only close to 1 $cm^{-3}\ s^{-1}$ as the onset nucleation rates. The data of this work lie below the data of Heist and Reiss (1973),[11] Mirabel and Katz (1977),[12] Chukanov and Kuligin (1987),[14] and of Brus *et al.* (2008).[32] It means that nucleation in this work occurs at lower saturation ratios than all data of others and fall just above the prediction of the CNT.[7] Experimental data of Wilson (1897) (Ref. 1) and Volmer and Flood (1934) (Ref. 3) sit on the dotted line symbolizing a perfect agreement with the CNT, while the data of Peters (1987) (Ref. 15) lies on the dotted line only at higher nucleation temperatures but deviates from it toward lower temperatures.

B. Comparison with the nucleation rate measurements

In order to compare the experimental data from all available techniques in a consistent manner and keep the picture as clear as possible we have chosen a scaled model of nucleation suggested by Hale.[42–44]

The so-called "Hale plot," see Fig. 8, produces two parameters $C_0[(T_c/T)-1]^3/(\ln S)^2$ and Ω. The first parameter accounts simultaneously for the temperature and supersaturation dependencies in the exponent of the nucleation rate expression. The parameter Ω is the excess surface entropy per molecule (divided by k), and is estimated from the experimental values of the surface tension. The effective value of Ω can be derived from C_0 by

$$\Omega=\left(\frac{3C_0}{16\pi}\times\ln 10\right)^{1/3}. \tag{2}$$

This method offers a way to check the experimental data for consistency and also provides a basis to compare the experi-

TABLE IV. The nucleation rates of water in helium. T_b is the temperature of the bottom plate, T_t is the temperature of the top plate, T_{nucl} is the nucleation temperature, p_{tot} is the total pressure, S_{nucl} is the supersaturation at T_{nucl}, N_{exp} is the measured flux of droplets, and J_{exp} is the experimental nucleation rate.

T_b (K)	T_t (K)	T_{nucl} (K)	p_{tot} (kPa)	S_{nucl}	N_{exp} (s^{-1})	J_{exp} ($\mathrm{cm}^{-3}\ \mathrm{s}^{-1}$)
			$T=295$ K, $p=80-85$ kPa			
342.37	276.75	295	80	3.591	21.88	1.49×10^{0}
341.89	276.64	295	80	3.554	14.52	8.82×10^{-1}
341.58	276.94	295	80	3.495	7.95	5.56×10^{-1}
341.32	277.17	295	80	3.448	3.21	2.49×10^{-1}
340.79	277.35	295	80	3.381	0.80	6.52×10^{-2}
340.33	277.56	295	80	3.318	0.13	1.14×10^{-2}
342.49	276.47	295	80	3.630	18.32	1.08×10^{0}
345.69	278.55	295	85	3.736	23.72	3.63×10^{0}
345.23	278.76	295	85	3.666	18.66	2.94×10^{0}
344.87	278.88	295	85	3.617	14.44	2.31×10^{0}
344.61	279.17	295	85	3.558	8.89	1.45×10^{0}
344.05	279.32	295	85	3.487	3.50	5.81×10^{-1}
343.72	279.60	295	85	3.425	1.29	2.14×10^{-1}
344.82	278.35	295	85	3.673	26.93	3.99×10^{0}
			$T=300$ K, $p=85$ kPa			
342.37	276.75	300	80	3.591	21.88	1.49×10^{0}
341.89	276.64	300	80	3.554	14.52	8.82×10^{-1}
341.58	276.94	300	80	3.495	7.95	5.56×10^{-1}
341.32	277.17	300	80	3.448	3.21	2.49×10^{-1}
340.79	277.35	300	80	3.381	0.80	6.52×10^{-2}
340.33	277.56	300	80	3.318	0.13	1.14×10^{-2}
342.49	276.47	300	80	3.630	18.32	1.08×10^{0}
			$T=305$ K, $p=90$ kPa			
356.40	288.70	305	90	3.191	21.78	3.57×10^{0}
355.97	288.97	305	90	3.137	15.33	2.61×10^{0}
355.73	289.22	305	90	3.098	7.97	1.39×10^{0}
355.28	289.33	305	90	3.058	4.43	7.83×10^{-1}
354.66	289.53	305	90	2.999	1.02	1.83×10^{-1}
354.47	289.75	305	90	2.967	0.31	5.53×10^{-2}
354.47	288.78	305	90	3.051	14.60	2.42×10^{0}
			$T=310$ K, $p=95$ kPa			
361.84	293.88	310	95	2.947	14.52	2.52×10^{0}
361.65	293.95	310	95	2.930	7.63	1.34×10^{0}
361.20	294.20	310	95	2.886	3.01	5.47×10^{-1}
360.70	294.53	310	95	2.832	1.00	1.87×10^{-1}
360.51	294.63	310	95	2.814	0.28	5.24×10^{-2}
360.08	294.85	310	95	2.773	0.11	2.06×10^{-2}
361.85	293.95	310	95	2.941	10.02	1.76×10^{0}
			$T=315$ K, $p=100$ kPa			
369.07	298.92	315	100	2.803	16.33	2.95×10^{0}
368.74	299.20	315	100	2.770	9.43	1.78×10^{0}
368.16	299.32	315	100	2.736	5.08	9.74×10^{-1}
367.86	299.57	315	100	2.705	1.72	3.37×10^{-1}
367.40	299.67	315	100	2.679	0.58	1.14×10^{-1}
367.00	299.82	315	100	2.651	0.24	4.75×10^{-2}
368.84	299.00	315	100	2.788	14.81	2.71×10^{0}
			$T=320$ K, $p=125$ kPa			
374.92	304.11	320	125	2.678	14.48	2.79×10^{0}
374.65	304.16	320	125	2.664	7.89	1.52×10^{0}
374.58	304.36	320	125	2.647	4.39	8.42×10^{-1}
373.64	304.51	320	125	2.600	1.78	3.41×10^{-1}

TABLE IV. (*Continued.*)

T_b (K)	T_t (K)	T_{nucl} (K)	p_{tot} (kPa)	S_{nucl}	N_{exp} (s^{-1})	J_{exp} (cm^{-3} s^{-1})
373.55	304.66	320	125	2.587	0.66	1.25×10^{-1}
373.19	304.96	320	125	2.552	0.33	5.90×10^{-2}
374.78	304.01	320	125	2.679	12.36	2.37×10^{0}

mental nucleation rates of any magnitude measured at arbitrary temperatures and supersaturations.

The Hale plot given on Fig. 8 uses the nucleation rate data of this work, Brus *et al.* (2008),[32] Miller *et al.* (1983),[23] Viisanen (1991),[25] Luijten *et al.* (1997),[27] Viisanen *et al.* (1993),[26] Wölk and Strey (2001),[29] Mikheev *et al.* (2002),[30] Holten *et al.* (2005),[31] and Heath *et al.* (2005).[18] The onset data are excluded from this comparison. The compared rates scale well over a wide range of temperatures and supersaturations and the experimental data from this work occurs on the top of the fit to all experimental data. The resulting value of the parameter C_0 is 23.6 and the effective value of Ω is 1.47. In the paper of Brus *et al.* (2008),[32] the data of Holten *et al.* (2005) (Ref. 31) were positioned wrongly on the Hale plot due to the mistake in data conversion. This was corrected in an Errata published recently.[45]

C. Critical cluster sizes

The critical cluster sizes can be calculated from the slopes of the nucleation rate isotherms according to the nucleation theorem:[46]

$$\left(\frac{\partial \ln J}{\partial \ln S}\right)_T \approx n^*. \tag{3}$$

In Eq. (3) n^* is the number of molecules in the critical cluster. One can also use the Kelvin equation to obtain the critical cluster radius r^*,

$$r^* = \frac{2\sigma v_{liq}}{kT \ln S}, \tag{4}$$

where v_{liq} is the volume of a liquid molecule and S is the experimental critical saturation ratio. According to the Kelvin equation, the critical cluster size depends both on the temperature and the saturation ratio. The number of molecules in the critical cluster determined from our experiments as a function of the number of molecules in the critical cluster predicted by Kelvin equation is presented in Fig. 9. Our measurements suggest a lower content of molecules in the critical cluster than suggested by theoretical prediction and are in good agreement with previous investigation of Brus *et al.* (2008).[32]

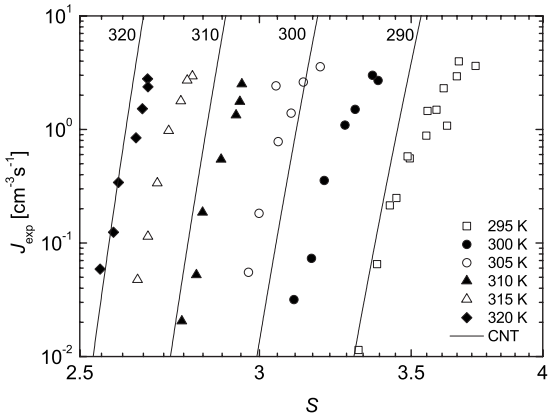

FIG. 5. The isothermal experimental nucleation rates of water, J_{exp}, as a function of its saturation ratio, S, in a comparison to CNT prediction.

IV. CONCLUSIONS

During the past decades the TDCC became a standard tool for nucleation research. However, it needed substantial improvements of the techniques determining the nucleation rate, and it also needed to satisfactorily resolve the problem of wetting chamber plates by the film of liquid water, before it was possible to measure the isothermal dependencies of nucleation rate on supersaturation in the supersaturated water vapor.

In this work we present results of a comparison, where the kinetics of homogeneous nucleation of water was studied independently in two laboratories using two different thermal diffusion cloud chambers, each using a qualitatively different method of determining the number of droplets formed by nucleation. In spite of this, a consistent picture of nucleation behavior resulted. The nucleation rate isotherms of water in helium are presented from 295 to 320 K with the step of 5 K, the nucleation rates ranged from 2×10^{-2} to 5×10^{1} cm^{-3} s^{-1}. The obtained experimental results are in a good agreement with previously published data and the pre-

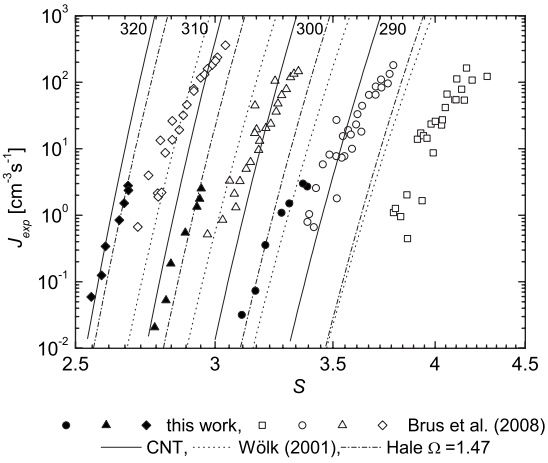

FIG. 6. The isothermal experimental nucleation rates of water, J_{exp}, of this work (solid symbols) as a function of saturation ratio, S, compared to data of Brus *et al.* (2008) (Ref. 32) (open symbols) and various theoretical predictions of nucleation rate: Classical nucleation theory (CNT) (Ref. 40), Wölk *et al.* (2002) (Ref. 41), and Hale scaled theory (Refs. 42–44) with $\Omega=1.47$.

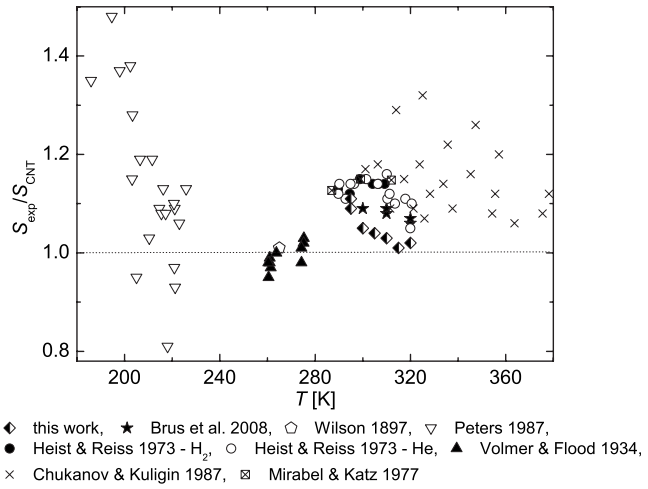

FIG. 7. Temperature dependence of the experimental saturation ratio to critical saturation ratio calculated by CNT.

diction of the classical nucleation theory (CNT). The experimental points are about factor of 2 higher to data of Brus *et al.* (2008) (Ref. 32) and lie just on top of the theoretical prediction of CNT corresponding to the isotherm 320 K. The data are also compared to the empirical nucleation rate function of Wölk *et al.* (2002).[41] The best agreement was found for Hale's scaled model[42–44] that fits well at all isotherms.

We also compare our data to the measurements of others, both to the onset data and to the nucleation rate measurements. Data of this work agree well with the onset data obtained from diffusion chambers in a similar temperature range. They occur at slightly lower saturation ratio than data of others and are just slightly above the prediction of the CNT. All available experimental nucleation rate data are compared in the so-called Hale plot. The experimental data from this work seems to be consistent with the data of others and the whole data set scales well over a wide range of temperatures and supersaturation ratios.

Critical cluster sizes were estimated from the slopes of measured isotherms and compared to the prediction of Kelvin equation. Our measurements suggest lower content of molecules in the critical cluster than the theoretical prediction; however our data are in good agreement with data of Brus *et al.* (2008).[32]

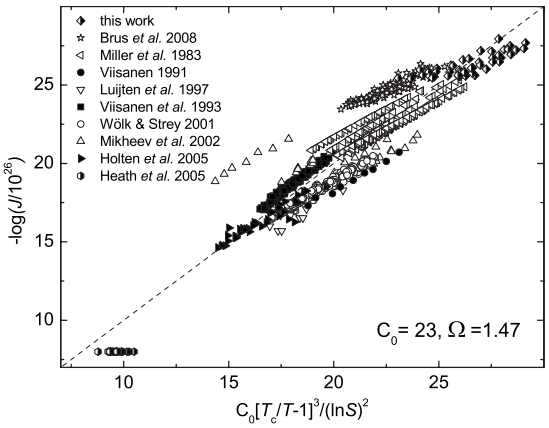

FIG. 8. A comparison of the scaled nucleation rates of water as a function of the scaled saturation ratio in the so-called Hale plot.

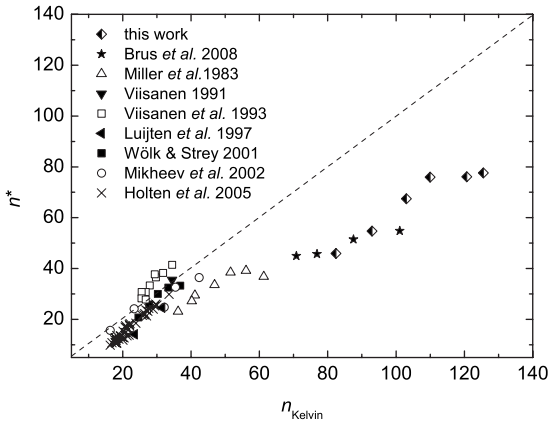

FIG. 9. Critical cluster sizes, determined from the slopes of experimental nucleation isotherms, compared to theoretical prediction by Kelvin equation.

Obtained results allow us to draw general conclusions on the methods of nucleation rate determination. The photographic method is more time consuming not only due to a smaller visible area given by the optical constraints but also due to the necessity to perform the subsequent image analysis. The main strength of the method is its independence on theory and also the possibility to check quality of the steady state using a detailed analysis of droplet trajectories, their shape and distribution. The photomultiplier method allows obtaining results more quickly and offers the experimentalist a faster feedback. With the coincidence counting technique it is possible to check the homogeneity of the droplets distribution in the chamber. The fact that the evaluated nucleation rates depend to some extent on the theory used seems to be of no importance. The present investigation showed that if the area visible by the photomultiplier is determined correctly, the results obtained by this method are quantitatively in agreement with the results determined by the photographic approach.

This comparative investigation is a critical review of the use of TDCCs in nucleation experiments. Many of the open questions could be answered:

Parameters individually optimized for each chamber as, for example, wall heating lead to identical results in nucleation rates. Different materials (aluminum and stainless steel) demonstrate the validity of the mathematical model used to calculate the chamber profiles. Only the slightly different temperature dependence of supersaturation at constant rate between our two measurements leaves an open question. This needs further investigation.

ACKNOWLEDGMENTS

The authors of this paper gratefully acknowledge the support by the Grant Agency of the Academy of Sciences of the Czech Republic, Grant No. IAA200760905.

[1] C. T. R. Wilson, Philos. Trans. R. Soc. London, Ser. A **189**, 265 (1897).
[2] C. F. Powell, Proc. R. Soc. London **A119**, 553 (1928).
[3] M. Volmer and H. Flood, Z. Phys. Chem. **A170**, 273 (1934).
[4] L. Scharrer, Ann. Phys. **35**, 619 (1939).
[5] A. Sander and G. Damkohler, Die Naturwissenschaften **31**, 460 (1943).
[6] L. A. Madonna, C. M. Sciulli, L. N. Canjar, and G. M. Pound, Proc. Phys. Soc. London **78**, 1218 (1961).

[7] J. L. Katz and B. J. Ostermier, J. Chem. Phys. **47**, 478 (1967).
[8] H. L. Jaeger, E. J. Wilson, P. G. Hill, and K. C. Rusell, J. Chem. Phys. **51**, 5380 (1969).
[9] G. D. Stein and C. A. Moses, J. Colloid Interface Sci. **39**, 504 (1972).
[10] D. Barschdorff, W. J. Dunning, P. P. Wegener, and B. J. C. Wu, Nature - Physical Science (London) **240**, 166 (1972).
[11] R. H. Heist and H. Reiss, J. Chem. Phys. **59**, 665 (1973).
[12] P. Mirabel and J. L. Katz, J. Chem. Phys. **67**, 1697 (1977).
[13] P. P. Wegener and C. F. Lee, J. Aerosol Sci. **14**, 29 (1983).
[14] V. N. Chukanov and A. P. Kuligin, Teplofiz. Vys. Temp. **25**, 70 (1987).
[15] F. Peters, J. Phys. Chem. **91**, 2487 (1987).
[16] G. Koppenwallner and C. Dankert, J. Phys. Chem. **91**, 2482 (1987).
[17] F. Peters and B. Paikert, Exp. Fluids **7**, 521 (1989).
[18] C. H. Heath, K. Streletzky, B. E. Wyslouzil, J. Wölk, and R. Strey, J. Chem. Phys. **117**, 6176 (2002).
[19] Y. J. Kim, B. E. Wyslouzil, G. Wilemski, J. Wölk, and R. Strey, J. Phys. Chem. A **108**, 4365 (2004).
[20] E. Allen and J. Kassner, J. Colloid Interface Sci. **30**, 81 (1969).
[21] G. D. Stein and J. A. Armstrong, J. Chem. Phys. **58**, 1999 (1973).
[22] P. E. Wagner and R. Strey, J. Phys. Chem. **85**, 2694 (1981).
[23] R. Miller, R. J. Anderson, J. K. Kassner, and D. E. Hagen, J. Chem. Phys. **78**, 3204 (1983).
[24] V. V. Beloded, G. A. Kirichewskij, and V. M. Nuzhnyi, J. Aerosol Sci. **20**, 1043 (1989).
[25] Y. Viisanen, "Experimental study of binary nucleation in the water n-propanol vapor mixture," Ph.D. thesis, Commentationes Physico-Mathematicae et Chemico-Medicae 133, 1991.
[26] Y. Viisanen, R. Strey, and H. Reiss, J. Chem. Phys. **99**, 4680 (1993).
[27] C. C. M. Luijten, K. J. Bosschaart, and M. E. H. van Dongen, J. Chem. Phys. **106**, 8116 (1997).
[28] C. C. M. Luijten, P. Peeters, and M. E. H. van Dongen, J. Chem. Phys. **111**, 8524 (1999).
[29] J. Wölk and R. Strey, J. Phys. Chem. B **105**, 11683 (2001).
[30] V. B. Mikheev, P. M. Irving, N. S. Laulainen, S. E. Barlow, and V. V. Pervukhin, J. Chem. Phys. **116**, 10772 (2002).
[31] V. Holten, D. G. Labetski, and van M. E. H. Dongen, J. Chem. Phys. **123**, 104505 (2005).
[32] D. Brus, V. Ždímal, and J. Smolík, J. Chem. Phys. **129**, 174501 (2008).
[33] V. Ždímal and J. Smolík, Atmos. Res. **46**, 391 (1998).
[34] D. C. Marvin and H. Reiss, J. Chem. Phys. **69**, 1897 (1978).
[35] C. H. Hung, M. J. Krasnopoler, and J. L. Katz, J. Chem. Phys. **90**, 1856 (1989).
[36] J. L. Katz, J. Chem. Phys. **52**, 4733 (1970).
[37] F. Stratmann, M. Wilck, V. Ždímal, and J. Smolík, J. Phys. Chem. B **105**, 11641 (2001).
[38] D. Brus, A.-P. Hyvärinen, V. Ždímal, and H. Lihavainen, J. Chem. Phys. **122**, 214506 (2005).
[39] M. Šonka, V. Hlaváč, and R. D. Boyle, *Image Processing, Analysis and Machine Vision* (PWS, Boston, 1998).
[40] R. Becker and W. Döring, Ann. Phys. (Leipzig) **24**, 719 (1935).
[41] J. Wölk, R. Strey, C. H. Heath, and B. E. Wyslouzil, J. Chem. Phys. **117**, 10 (2002).
[42] B. N. Hale, Phys. Rev. A **33**, 4156 (1986).
[43] B. N. Hale, Metall. Trans. A **23**, 1863 (1992).
[44] B. N. Hale, J. Chem. Phys. **122**, 204509 (2005).
[45] D. Brus, V. Ždímal, and J. Smolík, J. Chem. Phys. **130**, 219902 (2009).
[46] D. Kashchiev, J. Chem. Phys. **76**, 5098 (1982).